HIGH-ORDER STATE SPACE SIMULATION MODELS OF HELICOPTER FLIGHT MECHANICS

Frederick D. Kim
Roberto Celi
Department of Aerospace Engineering
University of Maryland, College Park, USA

Mark B. Tischler
U.S. Army Aeroflightdynamics Directorate
Ames Research Center, Moffett Field, USA

Abstract

This paper describes the formulation and validation of a high-order linearized mathematical model of helicopter flight mechanics, which includes rotor flap and lag degrees of freedom as well as inflow dynamics. The model is extracted numerically from an existing nonlinear, blade element, time simulation model. Extensive modifications in the formulation and solution process of the nonlinear model, required for a theoretically rigorous linearization, are described in detail. The validation results show that the linearized model successfully captures the coupled rotor-fuselage dynamics in the frequency band most critical for the design of advanced flight control systems. Additional results quantify the extent to which the order of the model can be reduced without loss of fidelity.

List of Symbols

C_T	Thrust coefficient
$[F]$	Linearized system matrix
g	Acceleration due to gravity
$[G]$	Linearized control matrix
p, q, r	Angular velocity components about body axes
r_D	Distance between hub and blade pickup for lag dampers
Δt	Integration step size
$[T]$	Transformation matrix from rotating to nonrotating coordinate system
u, v, w	Velocity components along body axes
$\mathbf{u}$	Control vector
V	Flight speed
$\mathbf{y}_{NR}$	State vector in nonrotating system
$\mathbf{y}_R$	State vector with rotor states in rotating system
β_k	Flap angle of k-th main rotor blade (rotating system)
β_0	Flap collective coordinate (nonrotating system)
β_{1c}, β_{1s}	Flap cyclic coordinates (nonrotating system)
β_2	Flap reactionless coordinate (nonrotating system)
ζ_k	Lag angle of k-th main rotor blade (rotating system)
ζ_0	Lag collective coordinate (nonrotating system)
ζ_{1c}, ζ_{1s}	Lag cyclic coordinates (nonrotating system)
ζ_2	Flap reactionless coordinate (nonrotating system)
θ_{DYN}	Main rotor blade angle of attack correction for elastic torsion
θ_G	Total pitch angle of main rotor blade
θ_t	Collective pitch of tail rotor
θ_0	Collective pitch of main rotor
θ_{1c}, θ_{1s}	Cyclic pitch components of main rotor
λ	Main rotor inflow
λ_H	State variable for wake effects on horizontal tail
μ	Advance ratio
μ_x, μ_y, μ_z	Components of advance ratio along x, y, and z body axes
ν	Total rotor downwash (nondimensional)
ϕ, θ, ψ	Fuselage attitudes (Euler angles)
ϕ_1, ϕ_2	State variables for the modeling of blade torsion
τ	Time constant for dynamic inflow
ψ	Blade azimuth angle
Ω	Main rotor speed

Subscripts

NR	Quantity in the nonrotating system
R	Quantity in the rotating system
$trim$	Value in trimmed condition
0	Collective mode in multiblade coordinates
$1c, 1s$	Cyclic modes in multiblade coordinates
2	Reactionless mode in multiblade coordinates

Other symbols

$\dot{(\,)}$	Derivative with respect to time
$\Delta(...)$	Small perturbation quantity

Introduction

The achievement of superior, mission-tailored handling qualities will be the driver for the new generation of military helicopters. The handling qualities requirements will depend on the specific mission, ranging from the precision flight control typical of nap-of-the-

Earth flying conditions, to the high maneuverability and agility required for air-to-air combat missions.

The need to satisfy the stringent handling qualities requirements of the future leads to highly coupled and unstable bare-airframe helicopter configurations such as high hinge offset, hingeless, or bearingless rotor configurations [1,2]. These helicopters will be equipped with high-gain, full-authority flight control systems to reduce off-axis cross-couplings, increase control bandwidth, and provide the desired response modes for given missions.

Because most modern multivariable control system design techniques require a linear mathematical model of the plant, the need exists for high quality linearized models of helicopter dynamics. It should be possible to extract these models from comprehensive, nonlinear helicopter flight simulation models. The dynamics of phenomena in the bandwidth of interest should be accurately modeled, therefore main rotor blade dynamics and inflow dynamics should be included in the linear model. In fact, neglecting rotor dynamics leads to greatly overpredicting the maximum gains that can be achieved in actual aircraft [3].

Motivated by the need for accurate linear models for flight control design applications, the activity in formulation and validation of high-order mathematical models of helicopter stability and control has increased in recent years. Only models capable of *predicting* the aircraft dynamics are considered in this section. Therefore no details are provided about the linear models obtained from flight test results, using system identification techniques. Mathematical models for the prediction of coupled rotor/fuselage aeromechanical instabilities such as ground and air resonance are also excluded from this discussion. Although these models have many of the ingredients required for stability and control analyses, the mathematical modeling of the fuselage dynamics is generally limited by the assumption that its motion be small. Extensive recent reviews of mathematical models for rotorcraft aeromechanics can be found in Refs. [4] and [5].

Zhao and Curtiss [6] have derived a set of linearized equations by analytic linearization of a nonlinear model formulated using Lagrange's equations. The computerized symbolic manipulation program MACSYMA was used for the formulation of both the nonlinear and the linearized model. The model includes 24 or 27 states depending on whether or not dynamic inflow is included. Flap and lag degrees of freedom are modeled in the nonrotating frame, using a multiblade coordinate transformation and retaining the collective and the first two cyclic modes for each degrees of freedom. Engine dynamics is not included. In forward flight, a flat vortex wake model is used to capture some of the effects of the main rotor wake on the tail surfaces and the tail rotor. The linear model is validated by comparing the predicted responses to step inputs of the various controls with flight test data, for both hover and forward flight conditions.

Another set of linearized equations is discussed by Schrage *et al.* [7]. The mathematical model implemented in the ARMCOP code [8], which contains the six rigid body degrees of freedom of the fuselage, three rotor flapping and the rotor speed degrees of freedom, was extended to include the flapping, lead-lag and dynamic inflow degrees of freedom, for a total of 15 degrees of freedom and 23 states. The linearization was partly performed analytically using MACSYMA, and partly numerically using finite difference approximations. The nonlinear model is validated by comparing predicted responses to step and impulse inputs of cyclic and collective pitch with flight test results. The linearized model, for which no validation results are presented in the paper, is used to carry out a study of the effects of model complexity on the poles of two helicopters. Results are presented for near hover and forward flight conditions.

Miller and White [9] formulate a nonlinear set of equations of motion in analytical form, using "Exponential Basis Functions" (EBF) to simplify the implementation of the sequence of coordinate transformations usually required in the formulation of coupled rotor-fuselage models. Through the use of EBF, a time-dependent coordinate transformation can be written as product of constant matrices and matrix exponentials. The latter can be multiplied by simple addition of the arguments, and can be differentiated easily. The equations of motion are formulated starting from Lagrange's equation, and a multiblade coordinate transformation is carried out to transform the rotor degrees of freedom into a nonrotating system. The nonlinear equations are linearized analytically. The total number of states is not mentioned explicitly, however rotor rigid body flap and lag degrees of freedom, as well as engine RPM and inflow dynamics are modeled, besides the fuselage rigid body degrees of freedom. Some validation results are presented. They include comparison of selected poles, and of time histories following longitudinal cyclic pitch inputs, with flight test results.

A linearized model based on the GENHEL code [10] is discussed by Diftler [11] in the context of an investigation of roll rate gain limitations for a stability augmentation system. A 13 degree of freedom model for fuselage, rotor flap and lag, rotor speed, and inflow is used with a total of 23 states. The linearizations are performed numerically by perturbing each of the states, and using finite difference approximations. Because of the peculiar implementation of the flight dynamics model in GENHEL, which will be discussed in the next section, the formulation of the perturbation scheme is not straightforward. The details of the procedure presented in the paper are rather sketchy, especially as to the coupling between the rotor and the fuselage degrees of freedom. No validation results are presented for the linearized model.

This model was subsequently extended to include the dynamics of an externally suspended load, and three elastic bending modes of the fuselage for a total of 42 states. Ref. [12] presents the results of a correlation study, in which frequency response plots obtained using both GENHEL, and the linearized model extracted from GENHEL, are compared with flight test data for a CH-53 helicopter. The region between 1 and 3 Hz emerges as the most critical, with rotor dynamics identified as a major possible cause of discrepancy between theory and experiment.

The main objective of this study is to formu-

late and validate a high-order linearized mathematical model of helicopter stability and control. This linear model is intended to be used in the design of advanced flight control systems based on new, powerful tools of multivariable feedback control system design. Because many of these tools are applied in the frequency domain, particular emphasis will be given to the validation of the linearized model through comparisons with *frequency response* data extracted from flight tests. The nonlinear simulation program GENHEL is used as the starting point for this study because this program is representative of the state of the art in helicopter simulation modeling, and because an extensive knowledge base has been developed in recent years, including comprehensive validation of the program with flight test results [13].

An additional objective of this study is to assess the accuracy of lower order linear models that may be extracted from the full size one. Because these models are expected to be used in the context of flight control system design, it is very important to determine what is the lowest order of the model that can be used reliably in the design process.

Mathematical model

Nonlinear mathematical model

The nonlinear mathematical model of the helicopter is based on the model originally implemented in the GENHEL computer program, as described in Ref. [10]. A series of modifications were carried out by Ballin [13], especially in the area of engine and drive train modeling, to improve the fidelity of the model. This upgraded version of GENHEL represented the starting point of the present study, and will be referred to in this paper as "GENHEL". The computer program that implements the modifications described in this section will be referred to as "UM-GENHEL".

A detailed description of the mathematical model implemented in GENHEL is beyond the scope of this paper, and only a brief outline is presented below. The fuselage is modeled as a rigid body. The rotor blades are individually modeled as rigid bodies undergoing flap and lag motion. Torsional deformations are taken into account approximately using a pseudo-modal approach with empirically derived modal coefficients. Rotor airmass dynamics is included. The aerodynamic forces on the rotor are calculated using blade element theory and quasi-steady aerodynamics. Airfoil lift and drag characteristics are provided in tabular form as functions of angle of attack and Mach number. The aerodynamic characteristics of fuselage and tail surfaces are also provided in tabular form, as functions of the angle of attack. In general, the model covers a wide range of angles of attack, sideslip, and inflow, and small angle assumptions are not invoked for fuselage attitudes and aerodynamic incidence angles.

The model includes a detailed description of the propulsion system; in the present study, however, main rotor speed was assumed to be constant, and not a degree of freedom. Furthermore, this study is concerned with the bare airframe dynamics, therefore the flight control system was assumed to be inoperative. Finally, it should be noted that although GENHEL is designed for real-time execution, no specific attempt to maintain this feature was made in modifying the computer program for the purpose of this study.

The mathematical model of the helicopter, as implemented in GENHEL, was not strictly in first-order, state variable form. Therefore a number of modifications were necessary in order to carry out a theoretically rigorous linearization. These modifications are described below.

Synchronization of solution

In GENHEL, the calculation of forces and moments acting on the helicopter at a given instant in time is conducted sequentially, with the equations of motion of the rotor being solved first, and the equations of motion of the fuselage being solved next [10]. Therefore, the calculation of the various portion of the right hand side of the ordinary differential equations (ODE) of motion is not performed simultaneously. It is possible that this lack of synchronization may cause inaccuracies in the solution, especially at higher frequencies, and introduce numerical phase lags. Furthermore, splitting the solution process complicates somewhat the task of perturbing the states, in order to obtain linearized information using finite difference approximations. Therefore, the first modification to GENHEL consisted in an extensive restructuring of the program, to bring together the solutions of the rotor and of the fuselage equations of motion so as to solve the entire system of ODE simultaneously.

Extraction of hidden states

The implementation of the mathematical model of the helicopter in GENHEL is such that the program contains a certain number of "hidden states", associated with the main rotor inflow dynamics, with the torsional dynamics of the main rotor blades, and with the modeling of the delay of wake effects on the tail surfaces and the tail rotor. The ODE describing the first two phenomena are solved using simple numerical schemes that are embedded in the calculation of the aerodynamic loads of the rotor. While not necessarily incorrect, this separate solution procedure relies on the facts that the integration step used to solve the ODE of rotor and fuselage is fixed, and that only one evaluation of the right hand side is performed at each integration step. This precludes the use of variable-step ODE solvers, and complicates greatly the use of ODE solvers that require more than one function evaluation per step. The delayed effects of the main rotor wake on the tail surfaces and the tail rotor are modeled through a pure time delay, expressed as a function of the (fixed) integration time step. Here the hidden states are those required to model approximately the time delay in state variable form.

A theoretically rigorous process of linearization requires that no hidden states be present, to avoid contamination of the linearized information. Therefore, another modification to GENHEL consisted in identifying and making explicit these hidden states. This was accomplished as follows:

1. GENHEL uses a cosine type approximation to the nonuniform inflow over the main rotor. The inflow dynamics is implemented numerically in

a discrete form of the type:

$$\lambda_{t+\Delta t} = f\left(\lambda_t, D_t, D_{t-\Delta t}, \Delta t\right) \qquad (1)$$

with

$$D_t = \frac{1}{2}\frac{C_T}{\sqrt{\mu_x^2 + \mu_y^2 + \lambda^2}} \qquad (2)$$

More precisely, the main rotor inflow λ is defined as the difference between the airflow velocity μ_z through the disk due to the advance ratio and the total downwash $\nu_{t-\Delta t}$ at the previous integration time step:

$$\lambda = \mu_z - \nu_{t-\Delta t} \qquad (3)$$

The downwash dynamics is described by the following equation:

$$\nu_t = C_1\nu_{t-\Delta t} + C_2 D_t + C_3 D_{t-\Delta t} \qquad (4)$$

where

$$C_1 = \exp\left(\frac{\mu\Delta t}{\tau}\right)$$

$$C_2 = \frac{C_1 + \frac{\mu\Delta t}{\tau} - 1}{\frac{\mu\Delta t}{\tau}}$$

$$C_3 = \frac{1 - C_1\left(1 + \frac{\mu\Delta t}{\tau}\right)}{\frac{\mu\Delta t}{\tau}}$$

The discrete form of Eq.(1) is reformulated in UM-GENHEL in the following continuous form:

$$\tau\dot{\nu} + \nu = \frac{1}{2}\frac{C_T}{\sqrt{\mu_x^2 + \mu_y^2 + \lambda^2}} \qquad (5)$$

with $\tau = 0.05$. The total inflow ν is added the vector of states, and the inflow λ is given by:

$$\lambda = \mu_z - \nu \qquad (6)$$

2. Blade torsion is taken approximately into account in GENHEL, using a pseudo-modal approach. First a tip dynamic twist θ_{DYN} is calculated in a form of the type:

$$\theta_{DYN}(t+\Delta t) = \\ = (C_1 + C_2\mu)\sum_{n=1}^{B}\sqrt{F_T^2(t) + F_P^2(t)} \qquad (7)$$

where B is the number of blades, C_1 and C_2 are empirically derived factors, and F_T and F_P are functions of the tangential and perpendicular forces acting on the blade. Then θ_{DYN} is multiplied by a torsion mode shape, to obtain a spanwise variation of dynamic twist which is applied identically to each rotor blade regardless of its azimuth angle.

Eq.(7) was made continuous by rewriting it in the following way:

$$\frac{\ddot{\theta}_{DYN}}{\omega_\theta^2\Omega^2} + \frac{2\zeta}{\omega_\theta\Omega}\dot{\theta}_{DYN} + \theta_{DYN} = \\ = (C_1 + C_2\mu)\sum_{n=1}^{B}\sqrt{F_T^2 + F_P^2} \qquad (8)$$

with $\zeta = 0.3$ and $\omega_\theta = 5.5$/rev. No attempt was made to modify the theory behind Eq.(7). Eq.(8) now introduces two extra states, namely:

$$\phi_1 = \theta_{DYN} \qquad \phi_2 = \dot{\theta}_{DYN}$$

3. The delay with which the main rotor downwash reaches the tail surfaces and the tail rotor is modeled in GENHEL in the form:

$$\nu_H(t) = \nu(t - n\Delta t) \qquad (9)$$

in which ν is the main rotor downwash, ν_H is the inflow at the tail, and $n\Delta T$ is the time the rotor downwash takes to reach the tail. This equation was modified with the substitution of the delay with an exponential lag:

$$\tau_H\dot{\nu}_H + \nu_H = \nu \qquad (10)$$

with $\tau_H = 0.001$. The modification introduced the explicit state λ_H.

Treatment of acceleration terms

In GENHEL, the equations of motion are implemented in the form:

$$\dot{\mathbf{y}} = \mathbf{g}\left(\dot{\mathbf{y}}, \mathbf{y}; t\right) \qquad (11)$$

that is, the vector $\dot{\mathbf{y}}$ appears both on the right and the left hand side of the equal sign. This form is due to the presence of body acceleration terms in the calculation of the inertia loads acting on the rotor blades, and complicates considerably a correct derivation of a set of linearized equations of motion.

A rigorous first-order form of the equations of motion was derived for implementation in UM-GENHEL. All the terms containing components of $\dot{\mathbf{y}}$ were identified, and Eq. (11) was rewritten in the form:

$$\dot{\mathbf{y}} = [E(t)]\dot{\mathbf{y}} + \mathbf{g}_1\left(\mathbf{y}; t\right) \qquad (12)$$

from which the required first-order form could easily be obtained as:

$$\dot{\mathbf{y}} = \left([I] - [E(t)]\right)^{-1}\mathbf{g}_1\left(\mathbf{y}; t\right) = \mathbf{f}\left(\mathbf{y}; t\right) \qquad (13)$$

Modeling of lag dampers

The forces generated by the lag damper are a nonlinear function of the axial velocity of compression or extension of the damper. The nonlinear force-velocity relationship is implemented through a table look-up procedure. The distance r_D between the hub pickup and the blade pickup is given by [10]:

$$r_D = f(\beta, \zeta, \theta_G) = \sqrt{X^2 + Y^2 + Z^2} \qquad (14)$$

with:

$$X = a\sin\beta + b\cos(\zeta+\zeta_0)\cos\beta + c + d\sin(\zeta+\zeta_0)\cos\beta \quad (15)$$

$$Y = -r\cos\theta_G - b\sin(\zeta+\zeta_0) + d\cos(\zeta+\zeta_0) \quad (16)$$

$$Z = a\cos\beta - r\sin\theta_G - b\sin\beta\cos(\zeta+\zeta_0) - d\sin\beta\sin(\zeta+\zeta_0) \quad (17)$$

where a, b, c, d, and r are known constants.

In GENHEL, the axial velocity $\dot{r}_D$ is computed using a finite difference approximation:

$$\dot{r}_D = \frac{f(\beta,\zeta,\theta_G)_t - f(\beta,\zeta,\theta_G)_{t-\Delta t}}{\Delta t} \quad (18)$$

that is implemented in such a way that the time step Δt must be fixed, and only one evaluation of the states β and ζ must be performed per time step. Therefore the modeling of the axial velocity of the damper introduces problems similar to those of the hidden states discussed previously.

In UM-GENHEL the dependence of $\dot{r}_D$ on states and controls at the previous time step is eliminated by deriving analytic expressions:

$$\dot{r}_D = \frac{1}{r_D}\left(X\frac{\partial X}{\partial t} + Y\frac{\partial Y}{\partial t} + Z\frac{\partial Z}{\partial t}\right) \quad (19)$$

The rate of change $\dot{\theta}_G$ of the blade pitch angle required to calculate $\dot{r}_D$ is given by:

$$\dot{\theta}_G = \dot{\theta}_0 + \left(\dot{\theta}_{1c} + \Omega\theta_{1s}\right)\cos\psi + \left(\dot{\theta}_{1s} - \Omega\theta_{1c}\right)\sin\psi \quad (20)$$

Modification of ODE solution algorithm

The equations of motion of the rotor in GENHEL are solved using a specially developed algorithm [10], based on the assumption that the blade motion is periodic. For example, for the flapping equation it is:

$$\dot{\beta}_t = \ddot{\beta}_{t-1}\frac{\sin\Delta\psi}{\Omega} + \dot{\beta}_{t-1}\cos\Delta\psi \quad (21)$$

$$\beta_t = \beta_{t-1} + \frac{\sin\Delta\psi}{\Omega}\dot{\beta}_{t-1} + \frac{1-\cos\Delta\psi}{\Omega^2}\ddot{\beta}_{t-1} \quad (22)$$

in which $\Delta\psi = \Omega\Delta t$. A similar solution scheme is used for the lag degree of freedom ζ. While the assumption of periodic motion is reasonable for a wide range of frequencies of interest in flight mechanics, it may be inaccurate for the fast, high frequency transients that can potentially occur in helicopters equipped with high-gain flight control systems.

The equations of motion of the fuselage are integrated in GENHEL by using a fixed-step scheme:

$$u_{n+1} = u_n + \Delta t\left(e_0\dot{u}_n + e_1\dot{u}_{n-1} + e_2\dot{u}_{n-2}\right) \quad (23)$$

used as a second order method with $e_0 = 3, e_1 = -1$, and $e_2 = 0$, or as a third order method with $e_0 = 3.602902, e_1 = -2.454456$, and $e_2 = 0.851554$. The Euler attitudes of the fuselage are obtained through an ad-hoc integration scheme, outlined here for the pitch attitude θ:

$$q_{n+1} = q_n + \Delta t\left(e_0\dot{q}_n + e_1\dot{q}_{n-1} + e_2\dot{q}_{n-2}\right) \quad (24)$$

$$r_{n+1} = r_n + \Delta t\left(e_0\dot{r}_n + e_1\dot{r}_{n-1} + e_2\dot{r}_{n-2}\right) \quad (25)$$

$$\dot{\theta}_{n+1} = q_{n+1}\cos\phi_n - r_{n+1}\sin\phi_n \quad (26)$$

$$\theta_{n+1} = \theta_n + \Delta t\left(e_0\dot{\theta}_n + e_1\dot{\theta}_{n-1} + e_2\dot{\theta}_{n-2}\right) \quad (27)$$

The modifications to GENHEL described previously make it simple to use general purpose ODE solvers. Therefore, both the special purpose solution algorithm for the rotor and the solution algorithm for the fuselage have been abandoned in UM-GENHEL, in favor of the sophisticated variable step, variable order Adams-Bashforth solver DE/STEP [14].

Transformation of rotor states into nonrotating coordinate system

Although not required for a correct solution of the equations of motion of the helicopter, it is customary to define the rotor states in a nonrotating coordinate system. In GENHEL, however, both the rotor states and the blade equations of motion are written in a rotating coordinate system. In order to minimize the differences between GENHEL and UM-GENHEL the equations of motion remain formulated in the rotating system, and the integration is conducted in the rotating system as well. However, at each integration step a multiblade coordination transformation can be performed, so that the output of the rotor states can be either in the rotating or the nonrotating system, depending on the user's choice.

The mathematical model in GENHEL is composed of a total of 17 degrees of freedom: 3 rigid body translations and 3 rigid body rotations for the fuselage, flap and lag angular motion for each of the four rigid blades plus a pseudo-torsion degree of freedom, inflow dynamics, and delay of downwash effects on the tail. The total number of states is 29, with the state vector defined as follows:

$$\mathbf{y}_R = [u\ v\ w\ p\ q\ r\ \phi\ \theta\ \psi\ \beta_1\ \beta_2\ \beta_3\ \beta_4\ \dot{\beta}_1\ \dot{\beta}_2\ \dot{\beta}_3\ \dot{\beta}_4\ \zeta_1\ \zeta_2\ \zeta_3\ \zeta_4\ \dot{\zeta}_1\ \dot{\zeta}_2\ \dot{\zeta}_3\ \dot{\zeta}_4\ \lambda\ \lambda_H\ \phi_1\ \phi_2]^T \quad (28)$$

The multiblade coordinate transformation of the flap degree of freedom for a four-bladed rotor yields four degrees of freedom: a collective β_0, two cyclic β_{1c} and β_{1s}, and a reactionless degree of freedom β_2 [15]. Similar results are obtained for the lag degree of freedom. The reactionless degrees of freedom don't affect directly the hub loads because they correspond to modes in which the resultant hub forces and moments are equal to zero, and are sometimes ignored on the analysis [6],[12]. However, they may affect the solution for the rotor motion, and for this reason they have been retained in the model. Thus, when the output of the rotor quantities is provided in the nonrotating system, the state vector becomes:

$$\mathbf{y}_{NR} = [u\ v\ w\ p\ q\ r\ \phi\ \theta\ \psi\ \beta_0\ \beta_{1c}\ \beta_{1s}\ \beta_2\ \dot{\beta}_0\ \dot{\beta}_{1c}\ \dot{\beta}_{1s}\ \dot{\beta}_2\zeta_0\ \zeta_{1c}\ \zeta_{1s}\ \zeta_2\ \dot{\zeta}_0\ \dot{\zeta}_{1c}\ \dot{\zeta}_{1s}\ \dot{\zeta}_2\ \lambda\ \lambda_H\ \phi_1\ \phi_2]^T \quad (29)$$

The vectors $\mathbf{y}_R$ and $\mathbf{y}_{NR}$ are related by:

$$\mathbf{y}_R = [T]\mathbf{y}_{NR} \tag{30}$$

where:

$$[T] = \begin{bmatrix} T_{11} & 0 & 0 \\ 0 & T_{22} & 0 \\ 0 & 0 & T_{33} \end{bmatrix}$$

and

$$T_{11} = [I] \qquad \text{(size 9 by 9)}$$

$$T_{22} = \begin{bmatrix} [T_f] & 0 \\ 0 & [T_f] \end{bmatrix}$$

$$T_{33} = [I] \qquad \text{(size 4 by 4)}$$

with

$$[T_f] = \begin{bmatrix} 1 & \cos\psi & \sin\psi & -1 \\ 1 & -\sin\psi & \cos\psi & 1 \\ 1 & -\cos\psi & -\sin\psi & -1 \\ 1 & \sin\psi & -\cos\psi & 1 \\ 0 & -\Omega\sin\psi & \Omega\cos\psi & 0 \\ 0 & -\Omega\cos\psi & -\Omega\sin\psi & 0 \\ 0 & \Omega\sin\psi & -\Omega\cos\psi & 0 \\ 0 & \Omega\cos\psi & \Omega\sin\psi & 0 \end{bmatrix}$$

$$\begin{bmatrix} 0 & 0 & 0 & 0 \\ 0 & 0 & 0 & 0 \\ 0 & 0 & 0 & 0 \\ 0 & 0 & 0 & 0 \\ 1 & \cos\psi & \sin\psi & -1 \\ 1 & -\sin\psi & \cos\psi & 1 \\ 1 & -\cos\psi & -\sin\psi & -1 \\ 1 & \sin\psi & -\cos\psi & 1 \end{bmatrix}$$

Linearized mathematical model

The main reason for the changes in formulation, solution, and implementation of the mathematical model described in the previous section was to cast the model in a rigorous first-order, state variable form of the type:

$$\dot{\mathbf{y}} = \mathbf{f}(\mathbf{y}, \mathbf{u}; t) \tag{31}$$

With the equations in the general form of Eq. (31), a linearized model suitable for flight control design applications can be obtained through a first order Taylor series expansion:

$$\Delta\dot{\mathbf{y}} = \left[\frac{\partial \mathbf{f}}{\partial \mathbf{y}}\right]_{\mathbf{y}=\mathbf{y}_{trim}} \Delta\mathbf{y} + \left[\frac{\partial \mathbf{f}}{\partial \mathbf{u}}\right]_{\mathbf{u}=\mathbf{u}_{trim}} \Delta\mathbf{u} + O\left(\| \Delta\mathbf{y} \|^2, \| \Delta\mathbf{u} \|^2\right) \tag{32}$$

with

$$\Delta\mathbf{y} = \mathbf{y} - \mathbf{y}_{\text{trim}} \tag{33}$$

$$\Delta\mathbf{u} = \mathbf{u} - \mathbf{u}_{\text{trim}} \tag{34}$$

Of course it is also:

$$\Delta\dot{\mathbf{y}} = \dot{\mathbf{y}} - \underbrace{\dot{\mathbf{y}}_{\text{trim}}}_{=0} = \dot{\mathbf{y}} \tag{35}$$

In the present study, the perturbation matrices in Eq. (32) are calculated using finite difference approximations. Therefore, the linearized model extracted from GENHEL has the form:

$$\Delta\dot{\mathbf{y}} = [F]\Delta\mathbf{y} + [G]\Delta\mathbf{u} \tag{36}$$

with:

$$[F] = \left[\frac{\partial \mathbf{f}}{\partial \mathbf{y}}\right]_{\mathbf{y}=\mathbf{y}_{trim}} \Delta\mathbf{y} \approx \left[\frac{\Delta \mathbf{f}}{\Delta \mathbf{y}}\right]_{\mathbf{y}=\mathbf{y}_{trim}} \Delta\mathbf{y} \tag{37}$$

$$[G] = \left[\frac{\partial \mathbf{f}}{\partial \mathbf{u}}\right]_{\mathbf{u}=\mathbf{u}_{trim}} \Delta\mathbf{u} \approx \left[\frac{\Delta \mathbf{f}}{\Delta \mathbf{u}}\right]_{\mathbf{u}=\mathbf{u}_{trim}} \Delta\mathbf{u} \tag{38}$$

The elements f_{ij} and g_{ij} in the i-th row and j-th column of $[F]$ and $[G]$ are respectively:

$$f_{ij} = \frac{f_i(\mathbf{y}_{trim} + \delta_j, \mathbf{u}_{trim}, t) - f_i(\mathbf{y}_{trim}, \mathbf{u}_{trim}, t)}{\delta_j}$$

$$g_{ij} = \frac{g_i(\mathbf{y}_{trim}, \mathbf{u}_{trim} + \delta_j, t) - g_i(\mathbf{y}_{trim}, \mathbf{u}_{trim}, t)}{\delta_j}$$

where δ_j is a vector with all its elements equal to zero, except for the j-th which is equal to a small number.

It should be noted that completely analytical formulations of the matrices of derivatives are impractical for mathematical models that make extensive use of look-up tables such as the one used in GENHEL. Furthermore, changes in selected portions of the mathematical model can be implemented much more easily when the derivatives are calculated numerically. These benefits were judged to outweigh the better physical insight offered by analytically derived $[F]$ and $[G]$ matrices.

The perturbations of the rotor degrees of freedom required to calculate the matrices $[F]$ and $[G]$ are applied in the rotating coordinate system. Therefore the notation $\mathbf{y}_R$ should be assumed throughout for the state vector in Eqs. (31) through (38). The linearized matrices, however, can be provided by UM–GENHEL entirely in the nonrotating system if required. The model then takes the form:

$$\Delta\dot{\mathbf{y}}_{NR} = [F_{NR}]\,\Delta\mathbf{y}_{NR} + [G_{NR}]\,\Delta\mathbf{u} \tag{39}$$

in which it is:

$$\Delta\mathbf{y}_{NR} = \mathbf{y}_{NR} - \mathbf{y}_{\text{NRtrim}} \tag{40}$$

$$\Delta\dot{\mathbf{y}}_{NR} = \dot{\mathbf{y}}_{NR} - \underbrace{\dot{\mathbf{y}}_{\text{NRtrim}}}_{=0} = \dot{\mathbf{y}}_{NR} \tag{41}$$

The perturbation matrices $[F_{NR}]$ and $[G_{NR}]$ in the nonrotating frame are obtained from the matrices $[F]$ and $[G]$ through the transformations

$$[F_{NR}] = [T]^{-1}\left([F][T] - [\dot{T}]\right) \tag{42}$$

$$[G_{NR}] = [T]^{-1}[G] \tag{43}$$

in which the coordinate transformation matrix $[T]$ is the same as in Eq. (30).

Finally the control vector $\Delta\mathbf{u}$ is defined as:

$$\Delta\mathbf{u} = \lfloor \theta_0 \; \theta_{1c} \; \theta_{1s} \; \theta_t \; \dot{\theta}_0 \; \dot{\theta}_{1c} \; \dot{\theta}_{1s} \; \dot{\theta}_t \; \rfloor^T \qquad (44)$$

All the components of the vector are to be intended as perturbations from the respective trim values. The presence of time derivatives in Eq. (44) is required for a correct modeling of the lag damper, Eqs. (19) and (20).

Reduced order linearized models

The reduced order models are generated by UM-GENHEL using the following algorithm. First, the linearized equations of motion are rearranged and partitioned as:

$$\left\{ \begin{array}{c} \Delta\dot{\mathbf{y}}_R \\ \Delta\dot{\mathbf{y}}_D \end{array} \right\} = \left[\begin{array}{cc} F_{RR} & F_{RD} \\ F_{DR} & F_{DD} \end{array} \right] \left\{ \begin{array}{c} \Delta\mathbf{y}_R \\ \Delta\mathbf{y}_D \end{array} \right\} \qquad (45)$$

where $\Delta\mathbf{y}_R$ and $\Delta\mathbf{y}_D$ are respectively the vector of states to be retained and to be discarded. Then the matrix products are expanded, and the vector $\Delta\dot{\mathbf{y}}_D$ is set equal to zero, to obtain:

$$\Delta\dot{\mathbf{y}}_R = F_{RR}\Delta\mathbf{y}_R + F_{RD}\Delta\mathbf{y}_D + G_R\Delta\mathbf{u} \qquad (46)$$

$$\Delta\dot{\mathbf{y}}_D = F_{DR}\Delta\mathbf{y}_R + F_{DD}\Delta\mathbf{y}_D + G_D\Delta\mathbf{u} = 0 \qquad (47)$$

The vector $\Delta\mathbf{y_D}$ can now be obtained in terms of $\Delta\mathbf{y_R}$ from Eq. (47) and substituted back into Eq. (46) to obtain the equations of motion for the reduced order model in matrix form:

$$\Delta\dot{\mathbf{y}}_R = \left(F_{RR} - F_{RD}F_{DD}^{-1}F_{DR}\right)\Delta\mathbf{y}_R + \left(G_R - F_{RD}F_{DD}^{-1}G_D\right)\Delta\mathbf{u} \qquad (48)$$

that can be rewritten more compactly as:

$$\Delta\dot{\mathbf{y}}_R = F_1\Delta\mathbf{y}_R + G_1\Delta\mathbf{u} \qquad (49)$$

Results

This section presents results that were derived to validate the UM-GENHEL computer code. As far as the nonlinear model is concerned, it should be emphasized that an improvement of the accuracy of UM-GENHEL, compared with GENHEL, was not one of the specific objectives of this study. Therefore the nonlinear portion of UM-GENHEL should be considered validated if the results show a good agreement with the original GENHEL. Such a validation was successfully conducted, although no results are presented in this paper. The linear portion of UM-GENHEL is the most important new contribution, and the main focus of this study. The validation of this portion consists in a comparison with the results obtained using the nonlinear version of GENHEL, and with flight test results. All the results presented in this section refer to a Sikorsky UH-60 helicopter in hover, with the flight control system turned off (bare airframe configuration).

Frequency domain validation

Figures 1 through 10 show frequency response plots for a hovering flight condition. The curves marked "Linearized UM-Genhel" indicate the results obtained using the linearized model described in this study. The curves marked "Non-Linear Genhel" were obtained from analytical results generated by the original GENHEL, through system identification techniques [16]. For these curves, as well as those obtained from flight test data (and correspondingly marked on the plots) the frequency band for which the identification is considered accurate is also indicated in the figures. This assessment is based on the evaluation of the coherence function γ_{xy}^2, defined as:

$$\gamma_{xy}^2 = \frac{|G_{xy}|^2}{|G_{xx}|\,|G_{yy}|} \qquad (50)$$

where G_{xx}, G_{yy}, and G_{xy} are respectively the input, output, and cross-spectral density estimates. A detailed discussion of the properties of the coherence function, as they pertain to the present study, can be found in Ref. [17]. The frequency response results presented in this section are considered accurate if the coherence function has a value

$$\gamma_{xy}^2 \geq 0.6$$

The comparison for the roll-rate response p to lateral cyclic input θ_{1c} is presented in Figures 1 and 2. As far as the amplitudes are concerned, between 2 and 10 rad/sec the linearized UM-GENHEL model performs as well as the identified model, and both show good agreement with flight test data. At lower frequencies UM-GENHEL reduces the overprediction compared with GENHEL, but exhibits a large peak corresponding to a lateral body mode of frequency $\omega_n = 0.529$ rad/sec and damping $\zeta = 0.014$. This peak is not shown either by the identified GENHEL model or by the flight tests. At higher frequencies, the UM-GENHEL again reduces the overprediction of the identified model, and captures slightly better the frequency of the notch response associated with the regressive lag mode, although the predicted drop in magnitude is greater. (The portion of the plot between the frequencies of 10 and 30 rad/sec is shown enlarged in Figure 3.) The phase responses are compared in Figure 2. Above 0.6 rad/sec, the two analytical models and the flight test show the same type of variation with frequency. The phase lag of the identified model is consistently higher than that of the flight tests, and a slight further increase is shown for UM-GENHEL. Below 0.6 rad/sec the phase predictions of the linearized UM-GENHEL are poor, and are again dominated by the lowly damped lateral body mode.

The amplitude and phase of the pitch rate responses q to longitudinal cyclic input θ_{1s} are compared in Figures 4 and 5 respectively. A very good agreement is shown in the prediction of amplitudes, for frequencies between 1 and 5-6 rad/sec, between both analytical models and the flight test results. At lower frequencies the two analytical models are fairly close, but both overpredict the response considerably. For frequencies above 5 rad/sec UM-GENHEL is in better agreement with flight tests than the identified model. Both analytical models predict much higher gains in the 16-20 rad/sec band around the natural frequency

of the lag regressive mode. The phase lag of the identified model is consistently higher than that of the flight tests, and a slight further increase is shown for UM–GENHEL. Large errors appear above 15 rad/sec, with UM–GENHEL improving rather substantially over the identified model.

The vertical response $\dot{w}$ to collective pitch input θ_0 is shown in Figures 7 and 8 for amplitude and phase respectively. The quality of the amplitude predictions of the two analytical models is comparable, with the UM–GENHEL model slightly underpredicting the gains at higher frequencies. On the other hand, rather large phase differences can be observed between the UM–GENHEL predictions and the flight test data, with phase delays larger by 20 to 40 degrees throughout the 0.5 to 10 rad/sec frequency band.

The amplitude of the yaw rate response r to tail rotor collective input θ_t predicted by the linearized UM–GENHEL is in the same or better agreement with flight tests than that predicted by the identified model, as shown in Figure 9. An improvement is especially noticeable in the phase response, shown in Figure 10. While UM–GENHEL does not capture accurately the sharp rises of magnitude and phase that occur at frequencies above 10 rad/sec, the agreement with flight data is substantially improved over that of the identified model.

Finally, the poles calculated using the linearized UM–GENHEL model are presented in Figure 11. A portion of the plot, which contains most of the fuselage poles, is shown enlarged in Figure 12. Frequency and damping of each mode are also presented in tabular form in Table 1.

Assessment of reduced order models

The primary objective of the work described in this paper was to derive a linearized simulation model of helicopter flight mechanics that was suitable for flight control system design applications. It is therefore important to determine what the lowest order of the model is that still describes the helicopter dynamics with sufficient accuracy. This section presents the initial results of a systematic study of reduced order models, obtained as described previously in the paper.

Frequency response plots of on-axis responses in roll, pitch, heave, and yaw are presented in Figures 13 through 20, for three models of decreasing order. The curves marked "Linearized UM–Genhel" refer to the results of the full-order, 29 state linearized model. The curves marked "UM–Genhel (21 states)" refer to a 21 state model obtained by removing the states describing dynamic twist (two), reactionless flap (two), reactionless lag (two), delayed effect of downwash on tail (one), and dynamic inflow (one). The corresponding state vector is therefore:

$$\mathbf{y}_{NR_{21}} = \lfloor u\ v\ w\ p\ q\ r\ \phi\ \theta\ \psi\ \beta_0\ \beta_{1c}\ \beta_{1s}\ \dot{\beta}_0\ \dot{\beta}_{1c}\ \dot{\beta}_{1s}\ \zeta_0\ \zeta_{1c}\ \zeta_{1s}\ \dot{\zeta}_0\ \dot{\zeta}_{1c}\ \dot{\zeta}_{1s}\ \rfloor^T$$

Finally, the curves marked "UM–Genhel (9 states)" refer to a simple six degree of freedom model, with quasi-steady representation of the rotor and no inflow dynamics. The state vector for this case is:

$$\mathbf{y}_{NR_9} = \lfloor u\ v\ w\ p\ q\ r\ \phi\ \theta\ \psi \rfloor^T$$

As expected, the 9-state model is inaccurate for frequencies above 1-2 rad/sec and does not capture the characteristics of the frequency response that are dominated by the rotor dynamics. Therefore this simplified model is inadequate for the design of high-gain flight control systems. The 21-state model, on the other hand, appears to have essentially the same accuracy as the 29-state model, with the partial exception of the vertical dynamics. It is reasonable to expect little or no effect from the deletion of the four states associated with the reactionless flap and lag modes because these modes generate zero net forces and moments on the rotor. The dynamic twist states have a natural frequency much higher than the frequencies of interest (see Table 1), and can also eliminated with negligible loss of accuracy. It should be kept in mind, however, that the six rotor states eliminated in the 21-state model may become important in flight conditions at the edges of the flight envelope, because they affect the rotor dynamics, and therefore the magnitude of dynamic stall and compressibility effects. The state corresponding to dynamic inflow should not be eliminated. Instead, the results presented in Ref. [16] clearly show that better agreement with flight test can be obtained by increasing the states to the three required by Pitt-Peters' dynamic inflow model [18].

Summary and Conclusions

A high-order linearized mathematical model of helicopter flight dynamics was formulated; this model describes both the fuselage and the rotor dynamics, and is therefore suitable for the design of advanced flight control systems based on modern multivariable control theory. The model was extracted from a state-of-the-art, nonlinear time domain simulation code. This study indicates that great care has to be exercised in applying perturbation schemes to such codes, and that the underlying theory must be fully understood. The solution of the equations of motion of the aircraft has to be conducted in a synchronized manner, and possible "hidden states" must be identified and made explicit. A number of modifications of the nonlinear computer code were carried out, to make its theoretical base more rigorous and sound.

The linearized model was validated by comparing its results in the frequency domain with those obtained from a linearized model extracted from the original GENHEL through parameter identification techniques, and with flight test results. The comparison shows that, in general, the linearized UM–GENHEL model performs as well as, or better than, the identified model. A slightly higher phase delay in the roll rate response, and a higher phase delay in the heave response, observed using the linearized UM–GENHEL, will require further study.

In conclusion, the results presented in this report indicate that UM–GENHEL, with its ability to provide both nonlinear and high-order linearized simulation capabilities, is a promising new tool for the design of advanced helicopter flight control system.

Acknowledgements

This work was funded by NASA Ames Research Center, through Joint Research Interchange NCA2-310. Mark Ballin's help in understanding some features of the GENHEL code is gratefully acknowledged.

References

[1] Key, D.L., and Hoh, R.H., "New Handling-Qualities Requirements and How They Can Be Met," *Proceedings of the 43rd Annual Forum of the American Helicopter Society*, St. Louis, Missouri, May 1987, pp. 975-990.

[2] Tischler, M.B., "Assessment of Digital Flight-Control Technology for Advanced Combat Rotorcraft," *Journal of the American Helicopter Society*, Vol. 34, (4), October 1989, pp. 66-76.

[3] Chen, R.T.N., and Hindson, W.S., "Influence of High-Order Dynamics on Helicopter Flight-Control Bandwidth," *Journal of Guidance, Control, and Dynamics*, Vol. 9, (2), 1986, pp. 190-197.

[4] Friedmann, P.P., "Rotary-Wing Aeroelasticity with Application to VTOL Vehicles," Paper AIAA-90-1115-CP, *Proceedings of the AIAA/ASME/ASCE/AHS 31st Structures, Structural Dynamics and Materials Conference*, Long Beach, California, 2-4 April 1990, Part 3, pp. 1624-1670.

[5] Chopra, I., "Perspectives in Aeromechanical Stability of Helicopter Rotors," *Proceedings of the American Helicopter Society National Specialists' Meeting on Rotorcraft Dynamics*, Arlington, Texas, November 1989, to appear in *Vertica*.

[6] Zhao, X., and Curtiss, H.C., "A Linearized Model of Helicopter Dynamics Including Correlation With Flight Test," *Proceedings of the Second International Conference on Rotorcraft Basic Research*, University of Maryland, College Park, MD, February 1988.

[7] Schrage, D.P., Peters, D.A., Prasad, J.V.R., Stumpf, W.F., and He, C.-J., "Helicopter Stability and Control Modeling Improvements and Verification on Two Helicopters," Paper No. 77, *Proceedings of the Fourteenth European Rotorcraft Forum*, Milano, Italy, September 1988.

[8] Talbot, P.D., Tinling, B.E., Decker, W.A., and Chen, R.T.N., "A Mathematical Model of a Single Main Rotor Helicopter for Piloted Simulation," NASA TM-84281, September 1982.

[9] Miller, D.G., and White, F., "A Treatment of the Impact of Rotor-Fuselage Coupling on Helicopter Handling Qualities," *Proceedings of the 43rd Annual Forum of the American Helicopter Society*, St.Louis, Missouri, May 1987, pp. 631-644..

[10] Howlett, J.J., "UH-60A Black Hawk Engineering Simulation Program–Volume II-Background Report," NASA CR-166310, December 1981.

[11] Diftler, M.A., "UH-60A Helicopter Stability Augmentation Study," Paper No. 74, *Proceedings of the Fourteenth European Rotorcraft Forum*, Milano, Italy, September 1988.

[12] Kaplita, T.T., Driscoll, J.T., Diftler, M.A., and Wong, S.W., "Helicopter Simulation Development by Correlation With Frequency Sweep Flight Test Data," *Proceedings of the 45th Annual Forum of the American Helicopter Society*, Boston, MA, May 1989, pp. 681-692.

[13] Ballin, M.G., "Validation of a Real-Time Engineering Simulation of the UH-60A Helicopter," NASA TM-88360, February 1987.

[14] Shampine, L.F., and Gordon, M.K., *Computer Solution of Ordinary Differential Equations—The Initial Value Problem*, W.H. Freeman & Co., San Francisco, 1976.

[15] Johnson, W., *Helicopter Theory*, Princeton University Press, 1980, pp.350-352.

[16] Ballin, M.B., and Dalang-Secrétan M.-A., "Validation of the Dynamic Response of a Blade-Element UH-60 Simulation Model in Hovering Flight," *Proceedings of the 46th Annual Forum of the American Helicopter Society*, Washington, DC, May 1990.

[17] Tischler, M.B., "Frequency-Response Identification of XV-15 Tilt-Rotor Aircraft Dynamics," NASA TM-89428 and USAAVSCOM TM 87-A-2, May 1987, pp. 33-39.

[18] Pitt, D.M., and Peters, D.A., "Theoretical Prediction of Dynamic Inflow Derivatives," *Vertica*, Vol. 5, 1981, pp. 21-34.

Mode type	Real part	Imaginary part	Frequency ω_n (rad/sec)	Frequency ω_n (/rev)	Damping ζ
Lateral	-0.043207	0			
Longitudinal	-0.93215	0			
Longitudinal	-6.9601	0			
Downwash	-18.187	0			
Downwash on Tail	-142.86	0			
Lateral	-0.22001	±0.0457	0.225	0.008	0.979
Longitudinal	0.10545	±0.37829	0.393	0.015	-0.269
Lateral	-0.0072755	±0.52892	0.529	0.020	0.014
Regressive Flap	-6.477	±2.3659	6.896	0.255	0.939
Collective Lag	-3.0779	±6.9107	7.565	0.280	0.407
Reactionless Lag	-7.9165	±3.6605	8.722	0.323	0.908
Regressive Lag	-3.699	±18.862	19.221	0.711	0.192
Collective Flap	-7.5054	±25.82	26.889	0.995	0.279
Reactionless Flap	-11.074	±25.448	27.753	1.027	0.399
Progressive Lag	-5.5555	±37.858	38.263	1.416	0.145
Progressive Flap	-11.163	±52.295	53.473	1.979	0.209
Dynamic Twist	-47.582	±159.92	166.849	6.175	0.285

Table 1: Poles of the helicopter in hover

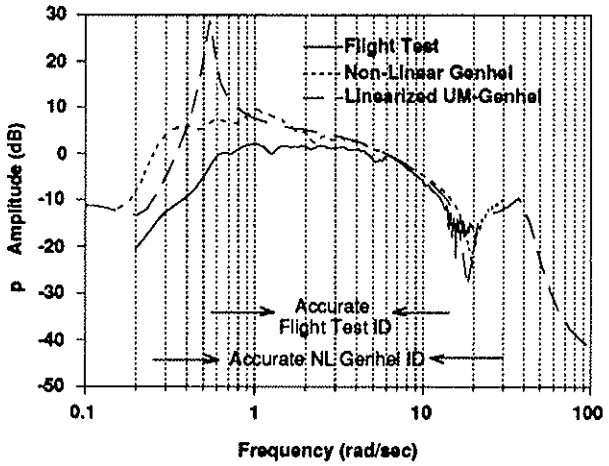

Figure 1: Bode amplitude plot of roll rate output p to lateral cyclic pitch input θ_{1c}.

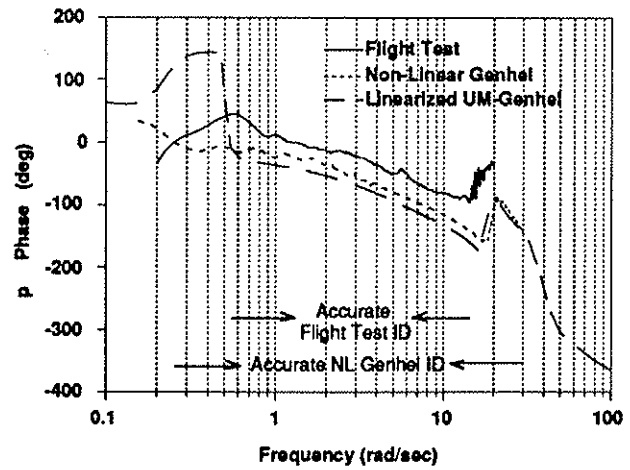

Figure 2: Bode phase plot of roll rate output p to lateral cyclic pitch input θ_{1c}.

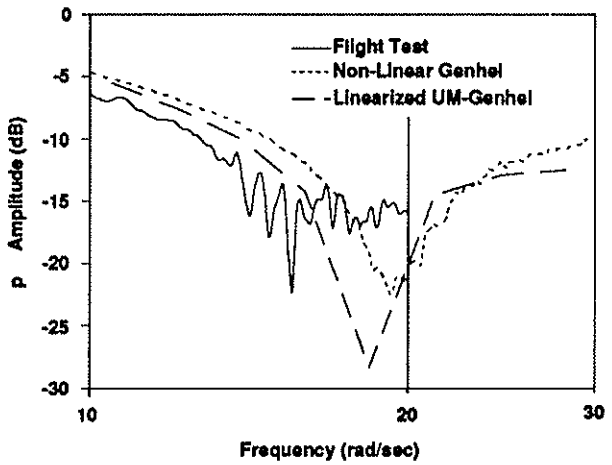

Figure 3: Detail of Bode amplitude plot of roll rate output p to lateral cyclic pitch input θ_{1c}.

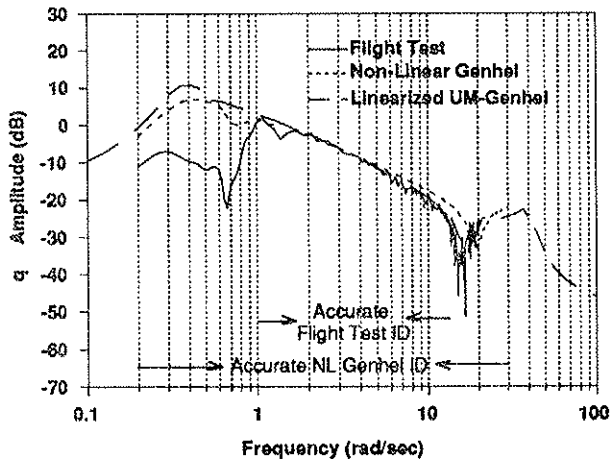

Figure 4: Bode amplitude plot of pitch rate output q to longitudinal cyclic pitch input θ_{1s}.

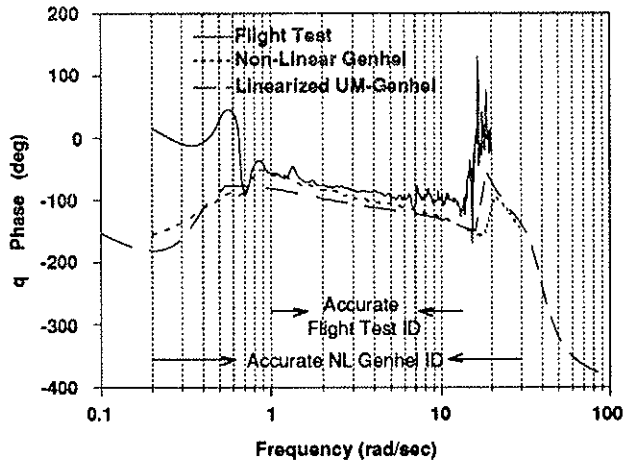

Figure 5: Bode phase plot of pitch rate output q to longitudinal cyclic pitch input θ_{1s}.

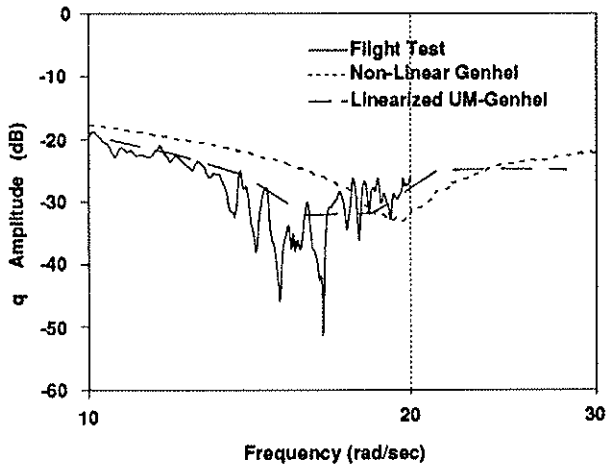

Figure 6: Bode amplitude plot of pitch rate output q to longitudinal cyclic pitch input θ_{1s}.

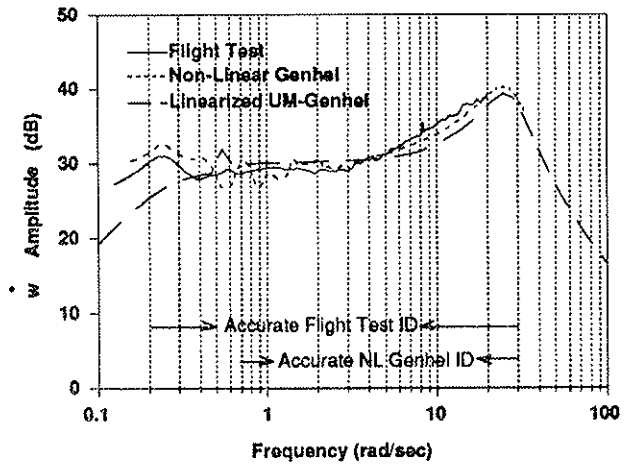

Figure 7: Bode amplitude plot of vertical acceleration output $\dot{w}$ to collective pitch input θ_0.

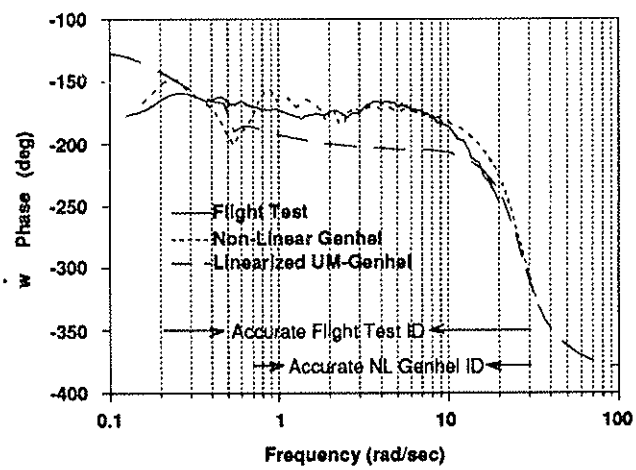

Figure 8: Bode phase plot of vertical acceleration output $\dot{w}$ to collective pitch input θ_0.

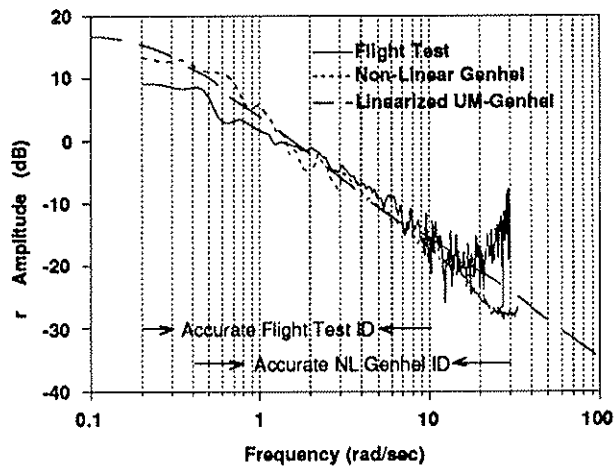

Figure 9: Bode phase plot of yaw rate output r to tail rotor collective pitch input θ_t.

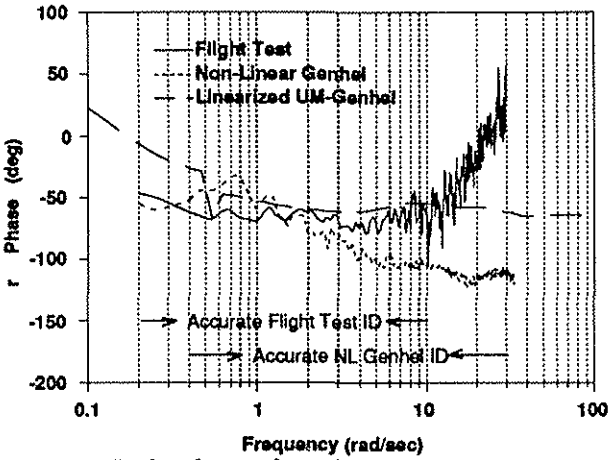

Figure 10: Bode phase plot of yaw rate output r to tail rotor collective pitch input θ_t.

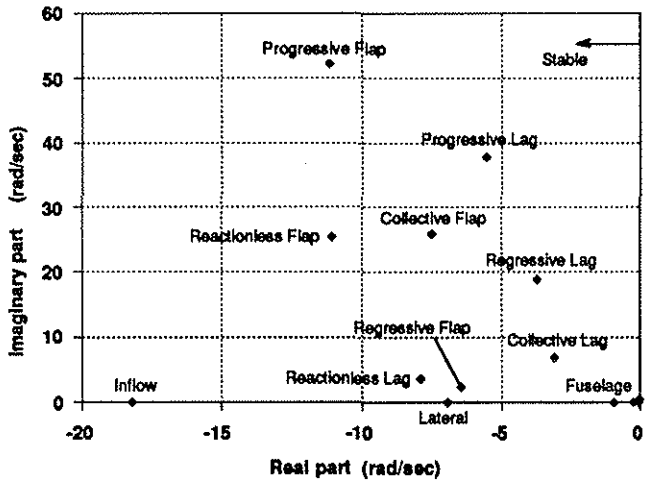

Figure 11: Poles of the helicopter

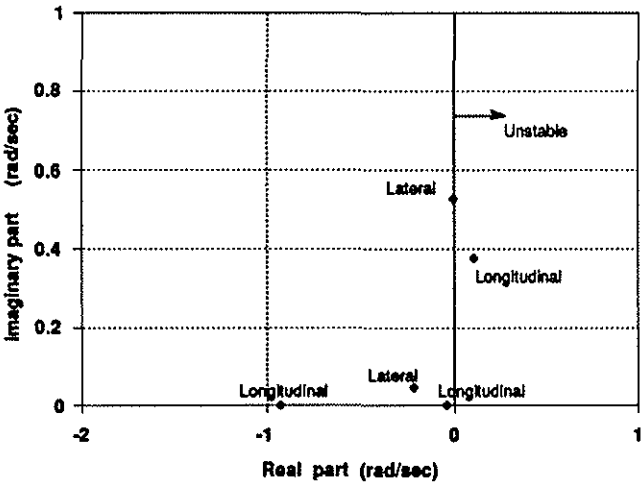

Figure 12: Poles of the helicopter—Detail of fuselage poles

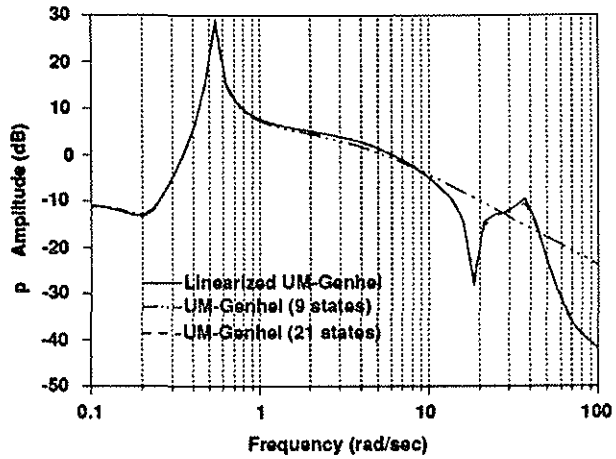

Figure 13: Bode amplitude plot of roll rate output q to lateral cyclic pitch input θ_{1c} for reduced order simulation models.

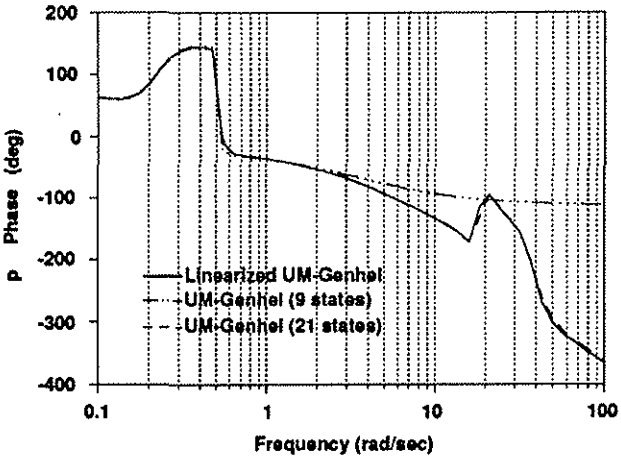

Figure 14: Bode phase plot of roll rate output q to lateral cyclic pitch input θ_{1c} for reduced order simulation models.

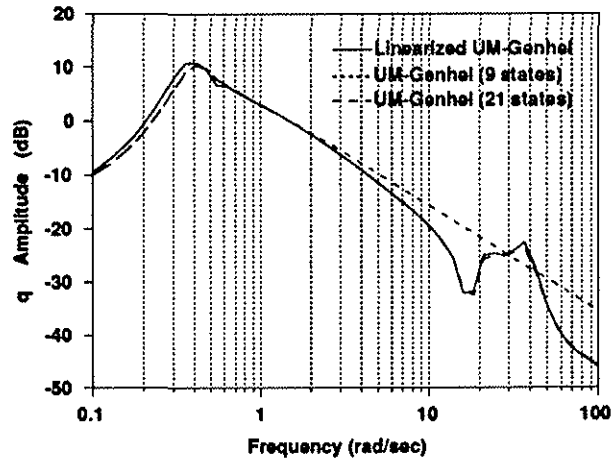

Figure 15: Bode amplitude plot of pitch rate output q to longitudinal cyclic pitch input θ_{1s} for reduced order simulation models.

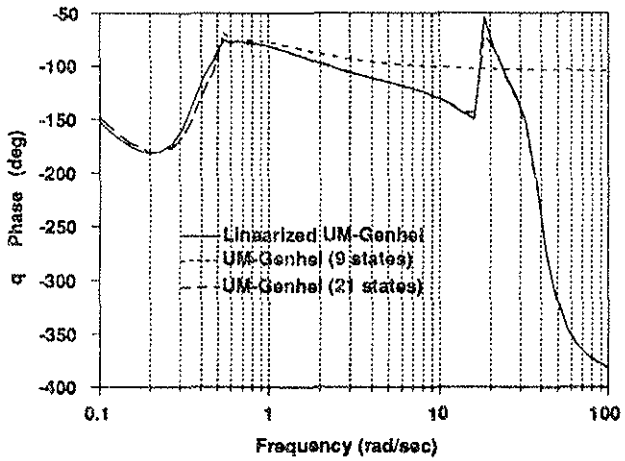

Figure 16: Bode phase plot of pitch rate output q to longitudinal cyclic pitch input θ_{1s} for reduced order simulation models.

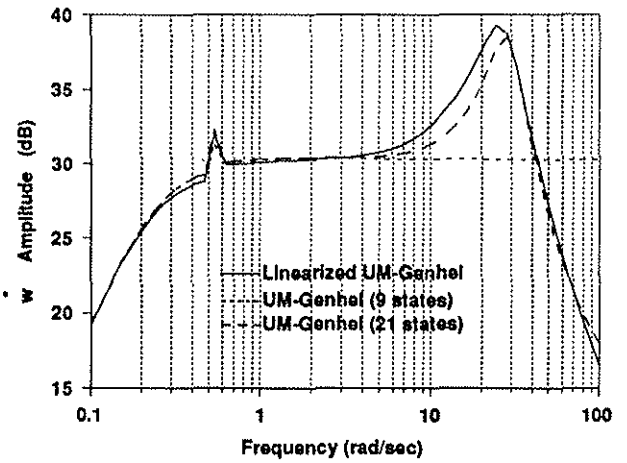

Figure 17: Bode amplitude plot of vertical acceleration output $\dot{w}$ to collective pitch input θ_0 for reduced order simulation models.

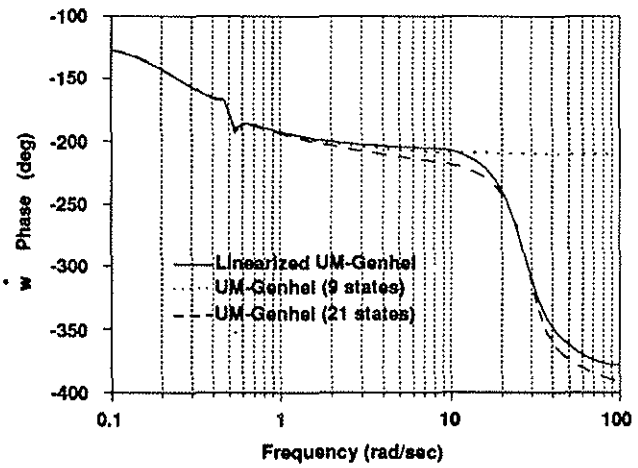

Figure 18: Bode phase plot of vertical acceleration output $\dot{w}$ to collective pitch input θ_0 for reduced order simulation models.

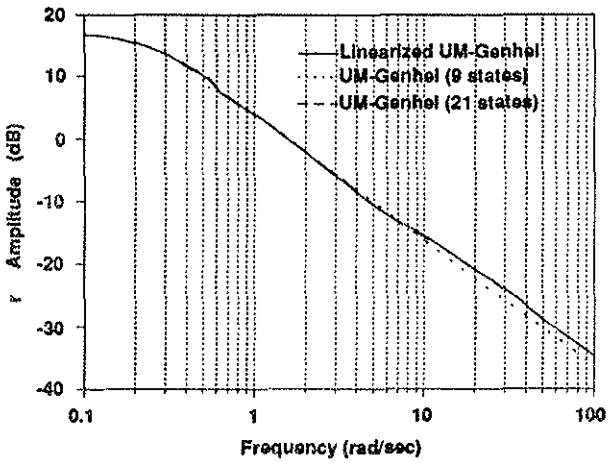

Figure 19: Bode phase plot of yaw rate output r to tail rotor collective pitch input θ_t for reduced order simulation models.

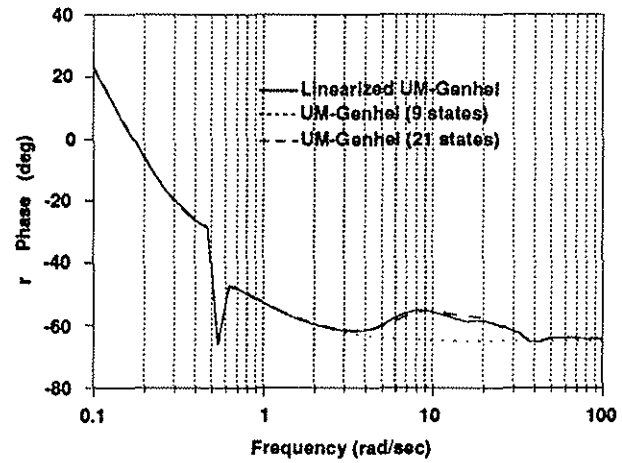

Figure 20: Bode phase plot of yaw rate output r to tail rotor collective pitch input θ_t for reduced order simulation models.